



**HAL**  
open science

# Disappearance of the Fe K $\alpha$ emission line in ultracompact X-ray binaries 4U 1543–624 and Swift J1756.9–2508

Filippos Koliopanos, Georgios Vasilopoulos, Sebastien Guillot, Natalie Webb

► **To cite this version:**

Filippos Koliopanos, Georgios Vasilopoulos, Sebastien Guillot, Natalie Webb. Disappearance of the Fe K  $\alpha$  emission line in ultracompact X-ray binaries 4U 1543–624 and Swift J1756.9–2508. Monthly Notices of the Royal Astronomical Society, 2020, 500 (4), pp.5603-5613. 10.1093/mnras/staa3490 . hal-02467229

**HAL Id: hal-02467229**

**<https://hal.science/hal-02467229>**

Submitted on 23 May 2024

**HAL** is a multi-disciplinary open access archive for the deposit and dissemination of scientific research documents, whether they are published or not. The documents may come from teaching and research institutions in France or abroad, or from public or private research centers.

L'archive ouverte pluridisciplinaire **HAL**, est destinée au dépôt et à la diffusion de documents scientifiques de niveau recherche, publiés ou non, émanant des établissements d'enseignement et de recherche français ou étrangers, des laboratoires publics ou privés.

# Disappearance of the Fe K $\alpha$ emission line in ultracompact X-ray binaries 4U 1543–624 and Swift J1756.9–2508

Filippos Koliopanos <sup>1</sup>★, Georgios Vasilopoulos <sup>2</sup>, Sebastien Guillot <sup>1</sup> and Natalie Webb <sup>1</sup>

<sup>1</sup>IRAP, Université de Toulouse, CNRS, CNES, 9 avenue du colonel Roche, BP 44346, F-31028 Toulouse, France

<sup>2</sup>Department of Astronomy, Yale University, PO Box 208101, New Haven, CT 06520-8101, USA

Accepted 2020 November 4. Received 2020 November 3; in original form 2020 January 2

## ABSTRACT

We investigate the long-term variability of the iron K  $\alpha$  line in the spectra of two ultracompact X-ray sources (UCXBs) with C/O-rich donors. We revisit archival observations from five different X-ray telescopes, over an  $\sim 20$ -yr period. Adopting physically motivated models for the spectral continuum, we probe the long-term evolution of the source emission in a self-consistent manner enabling physical interpretation of potential variability of the primary X-ray continuum emission and/or any emission lines from reflection off the accretion disc. We find that the spectral shape and flux of the source emission (for both objects) has remained almost constant throughout all the observations, displaying only minor variability in some spectral parameters and the source flux (largest variation is an  $\sim 25$  per cent drop in the flux of Swift J1756.9–2508). We note a striking variability of the Fe K  $\alpha$  line that fluctuates from a notable equivalent width of  $\sim 66$ – $100$  eV in 4U 1543–624 and  $\sim 170$  eV in Swift J1756.9–2508, to non-detections with upper limits of 2–8 eV. We argue that the disappearance of the iron line is due to the screening of the Fe K  $\alpha$  line by the overabundant oxygen in the C/O-rich UCXBs. This effect is cancelled when oxygen becomes fully ionized in the inner disc region, resulting in the variability of the Fe K  $\alpha$  line in an otherwise unaltered spectral shape. This finding supports earlier predictions on the consequences of H-poor, C/O-rich accretion disc on reflection-induced fluorescent lines in the spectra of UCXBs.

**Key words:** accretion, accretion discs – line: formation – radiative transfer – methods: observational – techniques: spectroscopic – X-rays: binaries.

## 1 INTRODUCTION

Ultracompact X-ray binaries (UCXBs) are accreting binary systems, defined by their very short (less than 1 h) orbital periods. Their periods suggest such tight orbits that a main sequence star cannot fit (e.g. Rappaport & Joss 1984; Nelson, Rappaport & Joss 1986). Evolutionary scenarios and observational findings indicate that UCXBs are composed of a Roche lobe filling white dwarf or helium star that is accreting material on to a neutron star (e.g. Tutukov & Yungelson 1993; Iben, Tutukov & Yungelson 1995; Verbunt & van den Heuvel 1995; Deloye & Bildsten 2003; Deloye, Bildsten & Nelemans 2005). More specifically, the different formation paths of UCXBs – which may or may not include a common envelope phase with their binary companion – result in donor stars that can range from He stars or He-WDs to C/O or O/Ne/Mg-WDs (e.g. Savonije, de Kool & van den Heuvel 1986; Podsiadlowski, Rappaport & Pfahl 2002; Yungelson, Nelemans & van den Heuvel 2002; Bildsten & Deloye 2004). For simplicity UCXBs are often divided into two main categories: He-rich and He-poor, depending on the donor composition. Since divergent UCXB formation paths lead to degenerate donors of similar mass, determining the chemical composition of the disc (and therefore the donor star) in these sources is a crucial step towards

constraining their formation history. Furthermore, UCXBs offer a unique opportunity to study accretion of hydrogen-poor matter on to compact objects.

The non-solar abundance of the accreting material in UCXBs can have a profound effect on the emission line spectrum of UCXBs in both the optical (He, C, or O lines; e.g. Nelemans et al. 2004; Nelemans, Jonker & Steeghs 2006; Werner et al. 2006) and the X-ray wavelengths (primarily in the form of C and O K  $\alpha$  lines; e.g. Juett, Psaltis & Chakrabarty 2001; Juett & Chakrabarty 2005; Madej et al. 2010). Nevertheless, due to the very faint optical counterparts of UCXBs ( $V$ -band absolute magnitudes  $\gtrsim 5$ ) but also due to the increased interstellar absorption in the  $< 1$  keV range of the X-ray spectrum, the detection of C and O emission lines is often considerably difficult. In a relatively recent theoretical study, Koliopanos, Gilfanov & Bildsten (2013) demonstrated that the iron K  $\alpha$  line located at 6.4 keV (and therefore not affected by interstellar absorption) can be used as an indirect method for determining the chemical composition of the accretion disc and donor star in UCXBs.

More specifically, for moderately luminous sources ( $L_X \lesssim$  a few  $10^{37}$  erg  $s^{-1}$ ) a strong suppression of the Fe K  $\alpha$  line was predicted in the case of a C/O or O/Ne/Mg WD donor, translating to a more than tenfold decrease of the equivalent width (EW) of the line. On the other hand, in the case of He-rich discs, the iron line remains unaffected with an EW in the same range as ‘standard’ X-ray binaries (XRBs) with hydrogen rich donors. Observational analysis of five well-

\* E-mail: [fkoliopanos@irap.omp.eu](mailto:fkoliopanos@irap.omp.eu)

known UCXB sources corroborated these predictions (Koliopanos et al. 2014). In addition to the above predictions, Koliopanos et al. (2013) indicated that the screening effect is decidedly linked to the ionization state of oxygen and (to a second degree) carbon. The authors further demonstrated that – given some specific assumptions – the ionization state of C and O in the disc and, subsequently, the presence or absence of the prominent Fe K  $\alpha$  line is luminosity dependent. In this paper, we report on the behaviour of two known UCXBs, which appear to exhibit the iron line variability, predicted by Koliopanos et al. (2013).

4U 1543–624 is a well-known UCXB that most likely hosts a C/O or Ne-rich WD donor (e.g. Juett et al. 2001). Discovered by the *UHURU* telescope (Jones 1977), it was classified as an UCXB after Wang & Chakrabarty (2004) established a period of  $P = 18.2$  min, based on optical light curves. 4U 1543–624 is a persistent X-ray source with a stable, moderately bright emission since its discovery. It has been observed by most major X-ray observatories, including *BeppoSAX* (Farinelli et al. 2003), *ASCA*, and *RXTE* (Schultz 2003) as well as *Chandra* and *XMM-Newton* (Juett et al. 2001; Juett & Chakrabarty 2003; Madej & Jonker 2011; Madej et al. 2014) and more recently *Neutron Star Interior Composition Explorer (NICER)*; this paper and Ludlam et al. 2019). The X-ray continuum of the source has been modelled using a variety of different models including thermal and non-thermal components leading to different interpretations for its physical origin. Furthermore, a pronounced emission line centred at  $\sim 0.7$  keV has been detected by both the *XMM-Newton* RGS and the *Chandra* HETG spectrometers. The emission line has been attributed to reflection of hard X-rays from a C/O-rich disc (most prominent being the O VII Ly  $\alpha$  line; e.g. Juett & Chakrabarty 2003; Madej & Jonker 2011; Madej et al. 2014). The presence of the iron K  $\alpha$  line – usually detected in the spectra of X-ray binaries – has been much more dubious. The line was reported in *BeppoSAX* and *RXTE* but was not present in *ASCA* spectra (Juett et al. 2001; Schultz 2003). Its potential presence has been tentatively claimed in the *XMM-Newton* spectra (Madej & Jonker 2011; Madej et al. 2014) but not in *Chandra* (Juett & Chakrabarty 2003). More recently, Ludlam et al. (2019) presented a thorough analysis of X-ray and radio observations of 4U 1543–624 during an enhanced accretion episode in 2017 (Ludlam et al. 2017; Miller et al. 2017). The iron emission line re-emerged during this phase; Ludlam et al. (2019) reported its presence and attributed it to X-ray reflection off the accretion disc surface.

Swift J1756.9–2508 is an LMXB located in the direction of the Galactic bulge. It was discovered in 2007 during an X-ray outburst observed by the *Swift*-BAT. Follow-up observations with *RXTE* identified the source as an UCXB ( $P_{\text{orb}} \sim 54.7$  min) with a millisecond pulsar (Krimm et al. 2007). The transient source was again detected by the *Swift*-BAT and *RXTE* Proportional Counter Array (PCA) during a second outburst in 2009 and more recently in 2018, when it was observed by *Swift*/XRT, *XMM-Newton*, *NuSTAR*, and *NICER* (Kuiper et al. 2018; Bult et al. 2018b). The multiple observations spanning more than a decade allowed the accurate study of the orbital evolution of the source (Patruno, Altamirano & Messenger 2010; Sanna et al. 2018; Bult et al. 2018a), which, in turn, indicated the strength of the NS magnetic field at  $\sim 2 \times 10^8$  G (Sanna et al. 2018). No type-I X-ray bursts were detected during any of the outbursts of Swift J1756.9–2508.

In this paper, we revisit observations of 4U 1543–624 and Swift J1756.9–2508 at different epochs, focusing our analysis on the shape of the spectral continuum and the presence or absence of the iron emission line. More specifically, we examine observations of 4U 1543–624 between 1997 and 2001 as well as its unusually

**Table 1.** List of observations of 4U 1543–624 and Swift J1756.9–2508 analysed in this paper.

Instrument	obsID	Date	Duration <sup>a</sup> (ks)
4U 1543–624			
<i>RXTE</i>	P20071	1997-05-06	14
<i>Chandra</i>	702	2000-09-12	30
<i>XMM-Newton</i>	0061140201	2001-02-04	50
<i>NICER</i>	1050060106	2017-08-20	13
Swift J1756.9–2508			
<i>RXTE</i>	P92050	2007-06-16	12
<i>XMM-Newton</i>	0830190401	2018-04-08	65
<i>NuSTAR</i>	90402313002	2018-04-08	40

<sup>a</sup>Duration of filtered observations.

bright 2017 outburst (4U 1543–624 is a persistent source, which entered a remarkably bright phase on 2017 September; Miller et al. 2017). For the transient source Swift J1756.9–2508, we study and compare its two outbursts of 2009 and 2018. We demonstrate that the X-ray spectrum of both sources has more or less the same shape through the years, which can be modelled using simple but physically motivated models. More importantly, we show that the flux of the Fe K  $\alpha$  emission detected on top of the continuum is variable by more than an order of magnitude. We discuss this behaviour in the context of our 2013 prediction for Fe line variability in C/O-rich UCXBs and utilize our findings to further scrutinize and extend our initial hypothesis.

## 2 OBSERVATIONS, DATA ANALYSIS AND RESULTS

In this work we revisit archival 1997 *RXTE*, 2000 *Chandra* high-energy transmission grating (HETG), 2001 *XMM-Newton* and 2017 *NICER* observations of 4U 1543–624 and 2009 *RXTE* and 2017 *XMM-Newton*/*NuSTAR* observations of Swift J1756.9–2508. Details of the observations are tabulated in Table 1. We note that in the case of the *RXTE* and *NICER* observations, there are multiple pointings within a period of several days during the source outburst. We have reviewed all available observations and selected those presented Table 1 based on their high number of registered counts. We have verified that within all data sets, the source was observed in the same spectral state. Analysis of the source spectra was carried out using the XSPEC X-ray spectral fitting package, Version 12.9.1 (Arnaud 1996).

### 2.1 Modelling the X-ray spectral continuum

In this analysis, we use a combination of multi-colour disc blackbody and nominal blackbody spectral components to model the X-ray emission continuum of our two sources. Our choice of the two thermal models is motivated by the expectation of an accretion disc that reaches all the way on to the NS surface on which it forms a layer of hot optically thick plasma. This assumption relies on long established theoretical considerations (e.g. Sunyaev & Shakura 1986; Sibgatullin & Sunyaev 2000) and a strong observational record of the presence of two thermal components in soft state NS-XRBs with low magnetic fields (e.g. Mitsuda et al. 1984; White, Stella & Parmar 1988; Mitsuda et al. 1989; Barret 2001; Lin, Remillard & Homan 2007; Revnivtsev, Suleimanov & Poutanen 2013).

Despite the simplicity of our spectral models, we are confident that their parameters describe actual physical characteristics of the

system (i.e. temperature and size of emitting regions). Therefore, we pay particular attention to the accuracy of fit derived values. We are particularly interested in the ionization state of the optically thick matter, while ensuring that the derived quantities are sensible in the context of accreting low magnetic field (low- $B$ ) NSs, i.e. temperature and inner disc radius commensurate with the size of the NS and the formation of the layer of hot ( $\gtrsim 1$  keV) optically thick plasma on its surface (e.g. Popham & Sunyaev 2001). For these reasons, it is important to take into account the effects of very high temperature ( $\gtrsim 10^6$  K) on the spectral shape of the thermal emission.

At this temperature range, most of the lighter elements in the upper disc layers will become fully ionized (see Section 3), resulting in an abundance of hot free electrons that significantly increase the impact of photon-electron scattering within the disc and boundary layer. The process modifies the blackbody spectrum, which – to the first approximation – appears ‘harder’ than it actually is. With respect to the spectral analysis – when modelling the continuum with typical thermal models such as `diskbb` or `bbodyrad` – our estimations of disc temperature and radius will deviate from their actual values. This issue is often called ‘spectral hardening’ and is usually addressed by applying a correction factor ( $f_{\text{col}}$ ) to the temperature and normalization of the thermal models (i.e. `diskbb` and `bbodyrad`; Lapidus, Syunyaev & Titarchuk 1986; London, Taam & Howard 1986; Shimura & Takahara 1995). Namely,

$$T_{\text{cor}} = \frac{T_{\text{in}}}{f_{\text{col}}} \quad (1)$$

and

$$R_{\text{cor}} = R_{\text{in}} f_{\text{col}}^2, \quad (2)$$

where  $T$  is the temperature of the MCD component and  $R_{\text{in}}$  is the inner radius. The value of  $f_{\text{col}}$  has been obsessively constrained between  $\sim 1.5$  and  $\sim 2.1$  (e.g. Zimmerman et al. 2005, and references therein). In the following analysis, we present all best-fitting values without correcting for the expected spectral hardening (i.e.  $f_{\text{col}} = 1.0$ ). The effects of a more realistic value of  $f_{\text{col}} \sim 1.8$  on the best-fitting estimated values of disc temperature and inner radius are discussed in Section 3.

## 2.2 X-ray spectroscopy of 4U 1543–624

### 2.2.1 XMM–Newton 2001 April observation

XMM–Newton observed 4U 1543–624 in 2001 April. All onboard instruments were operational. Namely, MOS1 and pn were operating in Timing Mode and MOS2 in Small Window Mode. All detectors had the Medium optical blocking filter on. In Timing mode, data are registered in one dimension, along the column axis, which results in significantly shorter CCD readout time (0.06 ms for Timing mode, instead of 5.7 ms of the Small Window mode). In addition to increased time resolution, the use of Timing mode may protect observations of bright sources from pile-up.<sup>1</sup>

**2.2.1.1 Spectral extraction and analysis** Spectra from all detectors were extracted using the latest XMM–Newton Data Analysis software SAS, version 15.0.0. and using the calibration files released<sup>2</sup> on May 12, 2016. All observations were checked for high background flaring

<sup>1</sup>For more information on pile-up, see <http://xmm2.esac.esa.int/docs/documents/CAL-TN-0050-1-0-ps.gz>.

<sup>2</sup>XMM–Newton CCF Release Note: XMM-CCF-REL-334.

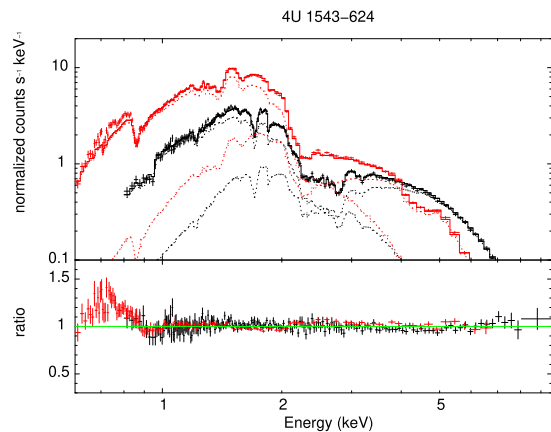


**Figure 1.** Normalized counts versus energy and ratio of the data to the continuum model for the 2000 *Chandra* observation. The data have been re-binned for clarity; the 1–10 keV energy range is shown.

activity. To this end, we extracted high energy light curves ( $E > 10$  keV for MOS and  $10 < E < 12$  keV for pn) with a 100-s bin size. A review of the lightcurves revealed no evidence of high energy flares in any of the detectors. The spectral extraction was done using SAS task `evselect`, with the standard filtering flags (`#XMEA_EP && PATTERN <= 4` for pn and `#XMEA_EM && PATTERN <= 12` for MOS). SAS tasks `RMFGEN` and `arfgen` were used to create the redistribution matrix and ancillary file. MOS2 data suffered from pile-up and, for this reason, they were rejected. Furthermore, because the effective area of pn at  $\sim 7$  keV is approximately five times higher than that of MOS and since the main interest of this work lies in this energy range, we opted to only use the pn data for our analysis. 4U 1543–624 is known to exhibit a complex emission and an absorption-like spectrum below 1 keV.

Several studies have indicated the presence of strong emission lines below 1 keV, as well as pronounced absorption edges, which are attributed to fluorescent emission and/or absorption from highly non-solar C/O or O/Ne/Mg-rich material transferred on to the NS by its degenerate donor (e.g. Juett et al. 2001; Juett & Chakrabarty 2003; Madej & Jonker 2011). The spectral models described in this section were applied to the entire energy range available from all detectors and we confirm the presence of soft emission-like features consistent with highly ionized oxygen. The emission-like feature is presented in Fig. 1 for the *Chandra* observation of 4U 1543–624 (i.e. normalized counts and data-to-model ratio versus energy, without accounting for the  $\sim 0.68$ -keV emission line reported by previous authors) and in Fig. 2 for the XMM–Newton data where again the broad emission-like feature and potential absorption edges are evident in the ratio plot. Modeling the residuals with a Gaussian emission line confirms the presence of a line centred at  $0.68 \pm 0.01$  keV with a width of  $70.9 \pm 0.25$  eV (in the 90 per cent confidence range). Nevertheless, the analysis of these features is not the focus of our study and since ignoring the energy channels below 1 keV simplifies our analysis without affecting our parameter estimations, all tabulated best-fitting values are for the spectral analysis of energy channels above 1 keV. This decision was made after confirming that the best-fitting values for the soft thermal component (`diskbb` model) are well constrained in the 1–10 keV range. Indeed, our broad-band analysis yielded  $kT_{\text{in}}$  and disc normalization values consistent, within the 90 per cent confidence range, with the 1–10 keV fit. The best-fitting values are also consistent within broadband models that include or omit the 0.68-keV Gaussian emission line. For a detailed study of

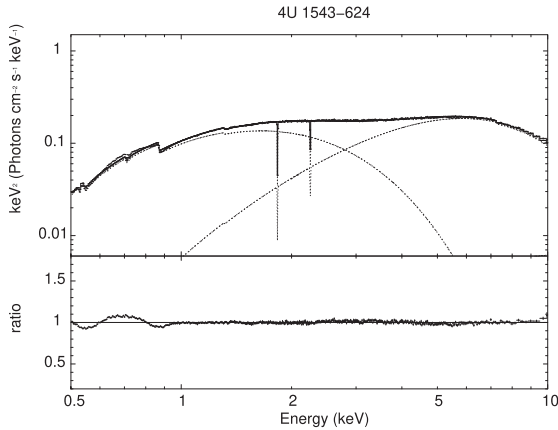


**Figure 2.** Unfolded spectrum versus energy and ratio of the data to the continuum model for the 2001 *XMM-Newton* observation. The data have been re-binned for clarity; the full 0.5–10 keV energy range is shown. The unfolded spectrum was chosen in order to visually demonstrate that the soft thermal component can be well constrained even if we ignore energy channels below 1 keV.

the atomic features and absorption edges in the low-energy part of the spectrum of 4U 1543–624, we refer the reader to the works of Juett & Chakrabarty (2003), Madej & Jonker (2011), and, most recently, Ludlam et al. (2019).

We fit the 1–10 keV spectral continuum with a combination of absorbed blackbody (XSPEC model `tbodyrad`) and disc blackbody (XSPEC model `diskbb`) components. The interstellar absorption was modelled using the improved version of the `tbabs` code<sup>3</sup> (Wilms, Allen & McCray 2000). The hydrogen column density ( $nH$ ) was frozen at the value provided by the HEASARC  $nH$  tool (HI4PI Collaboration et al. 2016). The fit yields a reduced  $\chi^2$  value of 1.04 for 1858/1795 d.o.f., and the data-to-model ratio plot does not indicate emission-like residuals in the entire 1–10 keV region (Fig. 3). Temperature of the disc blackbody is  $kT_{in} \sim 0.65$  keV and the blackbody temperature is  $kT_{BB} \sim 1.53$  keV. There is no evidence of iron  $K\alpha$  emission, with a  $1\sigma$  upper limit of 2.68 eV on the EW of the line. The source luminosity, extrapolated in the 0.50–30 keV range, is  $\approx 5.1 \times 10^{36}$  erg  $s^{-1}$ , for a distance of 7 kpc (Wang & Chakrabarty 2004). All values of the best-fitting parameters are presented in Table 2.

### 2.2.2 *RXTE* 1997 May observation

There are two *RXTE* observations of 4U 1543–624, both taken in 1997. The first observation commenced on May 5 and the second on September 22. Both observations were broken up into multiple intervals. We have analysed all available observations. However, for better clarity and brevity, we only present the results of the longest (14 ks) observation, taken on 1997 May 6 (P20071-04-01-00).

**2.2.2.1 Spectral extraction and analysis** *RXTE* had three onboard instruments: the All Sky Monitor (Levine et al. 1996), the PCA (Jahoda et al. 2006), and the High Energy X-ray Timing Experiment (HEXTE; Rothschild et al. 1998). In this work we obtain and analyse the source spectrum from the PCA, which provides the highest energy resolution (18 per cent at 6 keV) in the spectral range of interest (3–20 keV). The PCA detector is comprised of five proportional counter

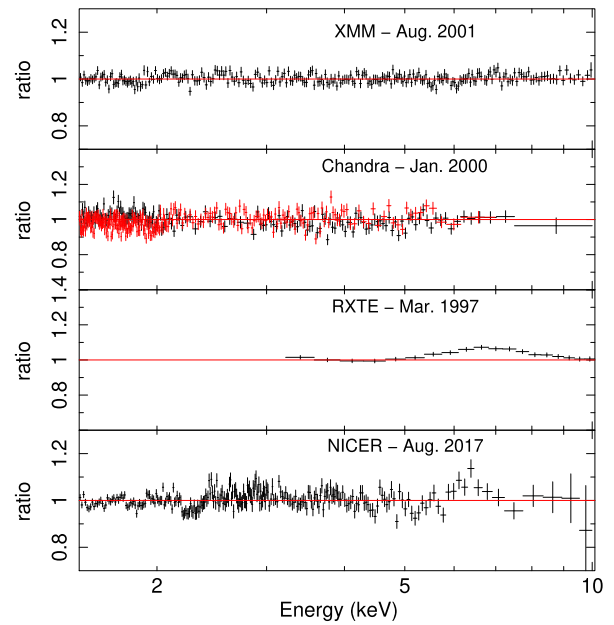


**Figure 3.** Data-to-model ratio plots for 4U 1543–624, illustrating the  $Fe K\alpha$  emission line variability through different epochs.

units (PCUs), with a combined effective area of  $\sim 7000$   $cm^2$ . Each PCU is composed of three layers of xenon (90 per cent) and methane (10 per cent) composites. Most incident photons with energies below 20 keV are detected in the top layer (layer 1) and, for this reason, we have opted to only extract spectra from this layer. All PCUs were active during the observation, which allowed us to obtain the data of all detectors for the spectral extraction. As per the recommendation<sup>4</sup> of the *RXTE* guest observer facility (GOF), we removed energy channels below 3 keV. Additionally, in our spectral extraction, we ignored all channels above 20 keV. The signal-to-noise ratio drops significantly above this threshold, and for this work we are primarily interested in the energy range below 20 keV. Due to the low orbit of *RXTE*, observations are occasionally affected by the satellite’s passage through the South Atlantic Anomaly (SAA) or by Earth occultation of the observed source. Data may also be affected by electron contamination and sporadic breakdowns of the PCU2 detector. For the spectral extraction, we filtered out intervals where the elevation angle was less than  $10^\circ$  (to avoid possible Earth occultations) and also any data that may have been received during passage from the SAA. Furthermore, we excluded any data affected by electron contamination, where offset by more than 0:02 or taken 150 s before, through 600 s after a PCU2 breakdown. Source spectra were extracted and background emission was modelled using standard routines from the `FTOOLS` package and the latest model for bright sources, provided by the GOF.<sup>5</sup> All spectra were re-binned to a minimum of 30 counts per bin.

The spectral continuum is again modelled with a similar combination of absorbed disc blackbody and blackbody emission, and a hydrogen column density ( $nH$ ) frozen at the Galactic value. The fit yields a reduced  $\chi^2$  value of 1.66 for 41 d.o.f., and the data-to-model ratio plot reveals strong positive residuals in the 6–7 keV region (Fig. 3). The residual structure – a strong indication of a bright

<sup>3</sup><http://pulsar.sternwarte.uni-erlangen.de/wilms/research/tbabs/>.

<sup>4</sup><https://heasarc.gsfc.nasa.gov/docs/xte/pca/doc/rmf/pcarmf-11.7/>.

<sup>5</sup>[http://heasarc.gsfc.nasa.gov/docs/xte/pca\\_news.html](http://heasarc.gsfc.nasa.gov/docs/xte/pca_news.html).

**Table 2.** Best-fitting parameters for the *XMM-Newton*, *Chandra*, *RXTE/PCA*, and *NICER* spectra of 4U 1543–624.

Model parameter	<i>RXTE-PCA</i> 1997 <sup>a</sup>	<i>Chandra</i> 2000	<i>XMM-Newton</i> 2001	<i>NICER</i> 2017
nH <sup>b</sup> ( $10^{22}$ cm <sup>-2</sup> )	0.29	0.29	0.29	0.29
<i>Disc blackbody</i>				
kT <sub>in</sub> (keV)	0.80 <sup>+0.31</sup> <sub>-0.22</sub>	0.71 <sup>+0.004</sup> <sub>-0.003</sub>	0.65 ± 0.02	0.79 <sup>+0.04</sup> <sub>-0.03</sub>
R <sub>in</sub> <sup>d</sup> (km)	9.02 ± 1.71	12.2 <sup>+0.30</sup> <sub>-0.26</sub>	13.6 <sup>+0.74</sup> <sub>-0.66</sub>	10.3 <sup>+0.54</sup> <sub>-0.42</sub>
<i>Blackbody</i>				
kT <sub>BB</sub> (keV)	1.81 <sup>+0.24</sup> <sub>-0.13</sub>	1.61 <sup>+0.04</sup> <sub>-0.03</sub>	1.53 <sup>+0.005</sup> <sub>-0.006</sub>	1.80 ± 0.02
Norm <sup>e</sup>	7.48 <sup>+0.27</sup> <sub>-0.98</sub>	7.00 ± 0.10	9.54 <sup>+0.79</sup> <sub>-0.76</sub>	4.26 ± 0.15
<i>Iron line</i>				
Centroid <i>E</i> (keV)	6.58 <sup>+0.21</sup> <sub>-0.33</sub>	6.6 <sup>f</sup>	6.6 <sup>f</sup>	6.47 ± 0.12
Width $\sigma$ (eV)	678 <sup>+131</sup> <sub>-121</sub>	500 <sup>f</sup>	500 <sup>f</sup>	160 <sup>+18.2</sup> <sub>-7.05</sub>
Flux <sup>g</sup>	95.1 <sup>+34.5</sup> <sub>-23.5</sub>	<5.05	<1.19	31.5 ± 5.7
EW (eV)	99.3 <sup>+36.6</sup> <sub>-24.3</sub>	<6.13	<2.68	61.3 ± 11.7
L <sub>Total</sub> <sup>h</sup>	6.65 ± 0.03	6.14 <sup>+0.09</sup> <sub>-0.08</sub>	5.14 ± 0.01	6.00 ± 0.01
L <sub>DBB</sub> <sup>h</sup>	1.56 <sup>+0.46</sup> <sub>-0.66</sub>	2.48 <sup>+0.32</sup> <sub>-0.10</sub>	2.78 ± 0.01	3.35 <sup>+0.18</sup> <sub>-0.12</sub>
L <sub>BB</sub> <sup>h</sup>	3.82 <sup>+0.64</sup> <sub>-0.44</sub>	3.76 ± 0.03	2.37 ± 0.01	2.54 ± 0.09
L <sub>BPL</sub> <sup>h</sup>	1.13 ± 0.14	–	–	–
$\chi^2$ /d.o.f.	16.9/38	3762/3703	1858/1795	807/743

*Note.* The errors are in the 90 per cent confidence range. <sup>a</sup>With an additional cutoff power law ( $\Gamma=2.49^{+0.17}_{-0.08}$  and  $E_{\text{cut}}=14.8^{+0.23}_{-0.85}$  keV), for the *RXTE* data.

<sup>b</sup>Parameter frozen at total galactic H I column density provided by the HEASARC nH tool (HI4PI Collaboration et al. 2016).

<sup>c</sup> $10^{-3}$  ph keV<sup>-1</sup> cm<sup>-2</sup> s<sup>-1</sup>.

<sup>d</sup>Solving  $K = (1/f_{\text{col}}^4)(R_{\text{in}}/D_{10\text{kpc}})^2 \cos i$ , for  $R_{\text{in}}$  (the inner radius of the disc in km).  $K$  is the normalization of the `diskbb` model,  $f_{\text{col}}$  is the spectral hardening factor,  $D_{10\text{kpc}}$  is distance in units of 10 kpc and  $i$  is the inclination. In the tabulated values, we have set  $f_{\text{col}} = 1$ .

<sup>e</sup> $(R_{\text{body}}/D_{10\text{kpc}})^2$ , where  $R_{\text{body}}$  is the size of the emitting region in km and  $D_{10\text{kpc}}$  is distance in units of 10 kpc.

<sup>f</sup>Parameters frozen. The centroid energy value was frozen at the median value of the 6.4–6.9 keV range, for a step of 0.1 keV and width value based on average width of observed Fe  $K\alpha$  emission lines in LMXBs (e.g. Cackett et al. 2009; Ng et al. 2010).

<sup>g</sup> $10^{-5}$  ph cm<sup>-2</sup> s<sup>-1</sup>.

<sup>h</sup>Luminosity in units of  $10^{36}$  erg s<sup>-1</sup>, extrapolated to the 0.50–30 keV range and assuming a distance of 7 kpc (Schultz 2003; Wang & Chakrabarty 2004).

iron  $K\alpha$  emission line – is modelled using a Gaussian. The high-energy range of *RXTE/PCA* ( $>10$  keV) allowed us to also probe the non-thermal tail of the 4U 1543–624 spectrum, which we modelled using a power law with a spectral index of  $\sim 2.5$  and a high energy exponential cutoff at  $\sim 15$  keV. The final fit yields a reduced  $\chi^2$  value of 0.44 for 38 d.o.f. (Fig. 4 for the 3–20 keV best-fitting plot). The temperature of the disc blackbody is  $kT_{\text{in}} \sim 0.8$  keV and for the blackbody is  $kT_{\text{BB}} \sim 1.8$  keV. The iron emission line is centred at  $\sim 6.58$  keV, has a width of  $\sim 670$  eV, and an EW of  $\sim 100$  eV. The source luminosity, extrapolated to the 0.50–30 keV range, is  $\approx 7.1 \times 10^{36}$  erg s<sup>-1</sup>. All values of the best-fitting parameters are presented in Table 2. Findings from the spectral analysis of the *XMM-Newton* observation (Section 2.2.1) and *RXTE* observation (Section 2.2.2) are also briefly presented in our comprehensive analysis of the entire UCXB catalogue in Koliopanos et al. (2020, accepted for publication in MNRAS).

### 2.2.3 Chandra 2000 December observation

The *Chandra* X-ray Observatory observed 4U 1543–624 four times. Once in December of 2000, using the HETG and three more times in June 2012, using the low energy transmission grating (LETG). Below we outline the spectral extraction and analysis for the 2000 HETG observation.

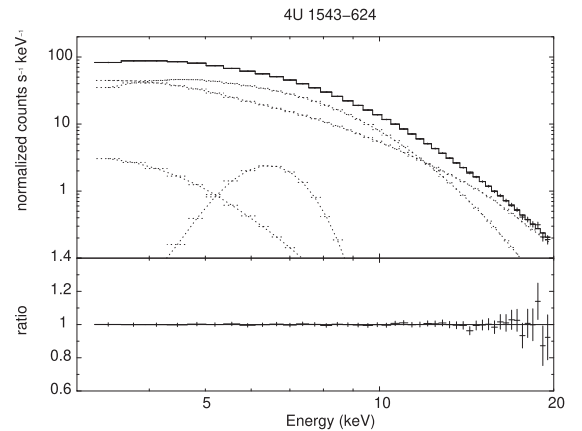


**Figure 4.** Normalized counts versus energy and ratio of the data to the continuum model for the 1997 *RXTE* observation. The data have been re-binned for clarity; the 3–20 keV energy range is shown.

**2.2.3.1 Spectral extraction and analysis** Using the tools included in the latest version of the CIAO software (vers. 4.8), we extract spectra from both the medium-energy grating (MEG) and the high-energy grating (HEG). Namely, upon selecting an appropriate extraction

region and taking into account the correct source position and telescope orientation during the entire observation, we use CIAO task `tgextract` to create a standard type II spectral file, containing all spectral orders of both the MEG and HEG detectors, and MKTGRESP to create their corresponding ancillary files and response matrices. In order to analyse the spectra with XSPEC, we create separate type I PHA files for the MEG and HEG spectra, simultaneously adding the +1 and -1 grating orders and rebinning them to a minimum of 30 counts per bin. We also create a separate background spectrum using the task `TG_BKG`.

The spectral continuum is well modelled with the same combination of absorbed disc blackbody and blackbody emission, as in the 1997 *RXTE* and 2001 *XMM-Newton* observations. The temperature of the disc blackbody lies at  $kT_{\text{in}} \sim 0.65$  keV and the blackbody temperature at  $kT_{\text{BB}} \sim 1.61$  keV. This time, no emission line was detected in the 6–7 keV range and we place a  $1\sigma$  upper limit for the EW of the iron  $K\alpha$  emission line at 6.13 eV. The double thermal model fit yielded a reduced  $\chi^2$  value of 1.02 for 3703 d.o.f (data-to-model ratio plot in Fig. 3). The source luminosity during the *Chandra* observation was  $\approx 6.1 \times 10^{36}$  erg s $^{-1}$ , calculated in the 0.50–30 keV range and assuming a distance of 7 kpc. All values of the best-fitting parameters are presented in Table 2.

#### 2.2.4 *NICER 2017 September observation*

4U 1543–624 was observed with *NICER* in 13 separate pointings over  $\sim 10$  d starting on 2017 August 15. Here we analyse obsID 1050060106, which, at a duration of  $\sim 13$  ks, provides the highest number of total counts after the standard event filtering described below.

**2.2.4.1 Spectral extraction and analysis** The *NICER* (Gendreau, Arzoumanian & Okajima 2012) operates on-board the International Space Station and consists of 56 ‘concentrator’ optics and silicon drift detector pairs registering X-ray photons in the 0.2–12 keV energy range. The 52 operating collectors comprise a total collecting area of  $\approx 1900$  cm $^2$  at 1.5 keV. *nicer*das 2018-10-07\_V005 was employed for the data reduction process. Namely, using NIMAKETIME, we created appropriate good time intervals (GTIs), by filtering out all raw data with the standard criteria using various housekeeping parameters (see Bogdanov et al. 2019; Guillot et al. 2019, for more details). The final event list was extracted using NIEXTRACT-EVENTS for PI energy channels between 40 and 1200, inclusive, and EVENT\_FLAGS = bxxx1x000 as per the *NICER* manual guidelines. For the spectral extraction, we used the HEASOFT tool XSELECT. The spectra were subsequently normalized based on the instrumental residuals calibrated from the Crab Nebula, as described in Ludlam et al. (2018).

The background spectrum was generated from a library of *NICER* observations of ‘blank sky’ fields (the same ones as for *RXTE*; Jahoda et al. 2006). Specifically, a weighted-average of these ‘blank sky’ observations with a similar combinations of observing conditions as our target’s data set is used to produce the diffuse cosmic X-ray background spectrum.<sup>6</sup> The latter is also normalized with the Crab Nebula residual spectrum. Finally, the latest ARF and RMF files were kindly provided by the *NICER* GOF (these are now publicly available as *NICER* XTI Calibration Files: 20200722 in the heasarc website).

<sup>6</sup>This background modeling technique is detailed in Bogdanov et al. (2019).

Observed by *NICER*, almost two decades after the *XMM-Newton* observations, the spectral continuum of 4U 1543–624 is qualitatively the same as in all previous observations and was again modelled with the same combination of absorbed disc blackbody and blackbody emission. The accretion disc temperature of the disc blackbody is closer to its value during the *RXTE* observation, at  $kT_{\text{in}} \sim 0.80$  keV as is the blackbody temperature that is estimated at  $kT_{\text{BB}} \sim 1.80$  keV. The iron  $K\alpha$  emission line has reappeared in the source spectrum, indicated by positive residual structure in the data-to-ratio versus energy plot in Fig. 3. The emission line was modelled with a Gaussian centred at  $\sim 6.5$  keV, with a width of  $\sim 160$  keV and an EW of  $\sim 61$  eV. The double thermal model including the Gaussian emission line yielded a reduced  $\chi^2$  value of 1.07 for 743 d.o.f. The source luminosity during the *NICER* observation was  $\approx 6.0 \times 10^{36}$  erg s $^{-1}$ , calculated in the 0.50–30 keV range and assuming the distance of 7 kpc. All values of the best-fitting parameters are presented in Table 2.

### 2.3 X-ray spectroscopy of Swift J1756.9–2508

#### 2.3.1 *RXTE 2007 June observation*

There are two sets of *RXTE* observations of Swift J1756.9–2508 carried out in 2007 when the source was first detected, and in 2009 during its second outburst. We have reviewed all available data and present here our analysis of the 2007 observation with the higher number of registered counts. For a thorough study of the entire *RXTE* observation campaign of Swift J1756.9–2508, we refer the reader to the works of Krimm et al. (2007) and Patruno et al. (2010).

**2.3.1.1 Spectral extraction and analysis** The extraction procedure for the *RXTE*/PCA spectra of Swift J1756.9–2508 is identical to the one described in subsection 2.2.2. The X-ray spectrum of Swift J1756.9–2508 during its 2007 outburst is also described by a combination of two absorbed thermal components, which is consistent with the high-luminosity soft-state spectra of weakly magnetized NS LMXBs (e.g. Lin et al. 2007). As expected for a source in the direction of the Galactic bulge, there is considerable interstellar absorption in the line of sight to Swift J1756.9–2508, with  $nH \sim 6 \times 10^{22}$  cm $^2$  (HI4PI Collaboration et al. 2016). The accretion disc temperature was estimated at  $kT_{\text{in}} \sim 1.1$  keV and the temperature of the blackbody component at  $kT_{\text{BB}} \sim 2.3$  keV. A prominent iron  $K\alpha$  emission line is clearly detected above the spectral continuum (see Fig. 5 for the data-to-model versus energy plot). The emission line is centred at  $\sim 6.5$  keV, and has an EW of  $\sim 171$  keV. The width of the emission line is smaller than the *RXTE*/PCA energy resolution (18 per cent at 6 keV) and was thus frozen to 500 eV. In addition to the thermal emission, the fit required a non-thermal component dominating  $> 10$  keV, which was modelled using a power law with spectral index of  $\Gamma \sim 1$  and a high-energy exponential cutoff at  $\sim 12$  keV. The model yields a reduced  $\chi^2$  value of 0.65 for 30 d.o.f. The source luminosity during the *RXTE* observation was  $\approx 5 \times 10^{36}$  erg s $^{-1}$ , calculated in the 0.50–30 keV range and assuming a distance of 8.5 kpc, based on the source position toward the direction of the Galactic Centre. All values of the best-fitting parameters along with errors in the 90 per cent confidence range are presented in Table 3.

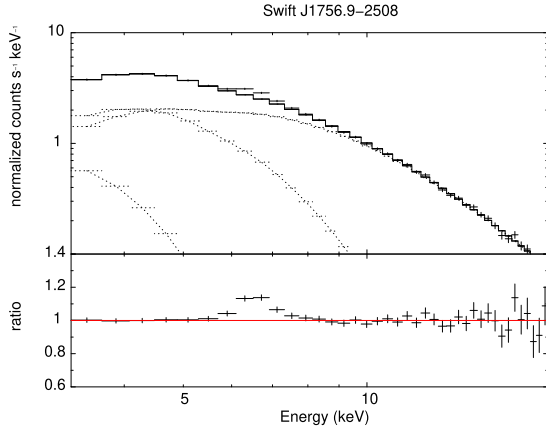


**Figure 5.** Normalized counts versus energy and ratio of the data to the continuum model for the 2007 *RXTE* observation Swift J1756.9–2508. The data have been re-binned for clarity; the 1–10 keV energy range is shown.

**Table 3.** Best-fitting parameters for the combined *NuSTAR*–*XMM*–*Newton* and *RXTE*/PCA spectra of Swift J1756.9–2508. The errors are 90 per cent.

Model parameter	<i>RXTE</i> /PCA 2007	<i>XMM</i> – <i>NuSTAR</i> 2018
$nH^a$ ( $10^{22}$ cm $^{-2}$ )	$6.05 \pm 1.02$	$7.28 \pm 0.07$
<i>Disc blackbody</i>		
$kT_{in}$ (keV)	$0.96^{+0.39}_{-0.18}$	$1.24^{+0.09}_{-0.06}$
$R_{in}^b$ (km)	$3.9^{+1.04}_{-1.66}$	$5.45^{+0.45}_{-0.42}$
<i>Blackbody</i>		
$kT_{BB}$ (keV)	$2.27^{+0.14}_{-0.09}$	$2.79^{+0.17}_{-0.12}$
Norm $^c$	$12.3^{+3.46}_{-6.53}$	$1.12 \pm 0.15$
<i>Cutoff power law</i>		
$\Gamma$	$0.97^{+0.22}_{-0.25}$	$1.39^{+0.07}_{-0.09}$
Norm ( $\times 10^{-3}$ )	$11.6^{+1.17}_{-0.77}$	$20.1^{+5.11}_{-4.89}$
$E_{cut}$ (keV)	$11.9^{+0.71}_{-0.69}$	$22.8^{+1.01}_{-0.68}$
$E_{fold}$ (keV)	$17.4^{+3.41}_{-2.67}$	$50.6^{+8.27}_{-6.38}$
<i>Iron line</i>		
Centroid $E$ (keV)	$6.47 \pm 0.12$	$6.6^d$
Width $\sigma$ (eV)	$500^d$	$500^d$
Flux $^e$	$42.3 \pm 4.5$	$<1.19$
EW (eV)	$171 \pm 18.5$	$<7.36$
$L_{Total}^f$ ( $\times 10^{36}$ erg s $^{-1}$ )	$4.87 \pm 0.10$	$3.67 \pm 0.02$
$L_{DBB}^f$ ( $\times 10^{36}$ erg s $^{-1}$ )	$0.84 \pm 0.11$	$0.91 \pm 0.07$
$L_{BB}^f$ ( $\times 10^{36}$ erg s $^{-1}$ )	$1.00 \pm 0.12$	$0.67 \pm 0.04$
$L_{cPL}^f$ ( $\times 10^{36}$ erg s $^{-1}$ )	$3.13 \pm 0.12$	$2.59 \pm 0.25$
$\chi^2/d.o.f.$	19.6/30	3255/3141

Notes.  $^a 10^{-3}$  ph keV $^{-1}$  cm $^{-2}$  s $^{-1}$ .

$^b$  Solving  $K = (1/f_{col}^4)((R_{in}/D)_{10kpc}^2 \cos i)$ , for  $R_{in}$  (the inner radius of the disc in km).  $K$  is the normalization of the *diskbb* model,  $f_{col}$  is the spectral hardening factor (again for the tabulate values  $f_{col} = 1$ ),  $D_{10kpc}$  is distance in units of 10 kpc, and  $i$  is the inclination.

$^c (R_{bbody}/D_{10kpc})^2$ , where  $R_{bbody}$  is the size of the emitting region in km and  $D_{10kpc}$  is distance in units of 10 kpc.

$^d$  Parameters frozen. The centroid energy value was frozen at the median value of the 6.4–6.9 keV range, for a step of 0.1 keV and width value based on average width of observed Fe  $K\alpha$  emission lines in LMXBs (e.g. Cackett et al. 2009; Ng et al. 2010), for the *RXTE* detection, the width is frozen at the instrument’s energy resolution at 6 keV. The two values coincide.

$^e 10^{-5}$  ph cm $^{-2}$  s $^{-1}$ .

$^f$  Luminosity extrapolated to the 0.50–30 keV range and assuming a distance of 8.5 kpc, based on the proximity toward the direction of the Galactic Centre.

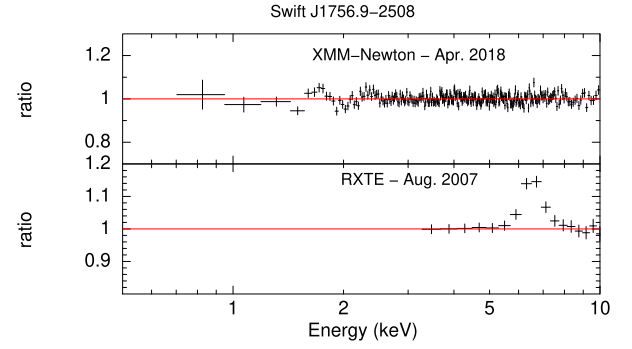


**Figure 6.** Data-to-model ratio plots for Swift J1756.9–2508, illustrating the Fe  $K\alpha$  emission line variability through different epochs.

### 2.3.2 XMM–Newton/*NuSTAR* 2018 April observation

Swift J1756.9–2508 was jointly observed with *XMM*–*Newton* and *NuSTAR* X-ray telescopes during its third and latest outburst in 2018 April.

**2.3.2.1 Spectral extraction and analysis** During the *XMM*–*Newton* observation of Swift J1756.9–2508, the EPIC-pn detector was again operated in Timing mode and therefore the spectral extraction process is the same as in 4U 1543–624 (paragraph 2.2.1). For the *NuSTAR* data extraction, we used version 1.9.3 of the *NuSTAR* data analysis system (*NuSTAR* DAS) and the latest instrumental calibration files from CalDB v20191008. Data were cleaned and calibrated using the NUPipeline routine with default settings. The internal high-energy background was reduced and passages through the South Atlantic Anomaly were screened (settings SAACALC = 3, TENTACLE = NO, and SAAMODE = OPTIMIZED). Phase-averaged source and background spectra were extracted using the NUPRODUCTS script, which also produces the instrumental responses for both focal plane modules, FPMA and B. We used a circular extraction region with an 80 arcsec radius for both the source and the background spectra. The latter were extracted from a blank sky region in the same detector as the source and at an adequate distance from it in order to avoid any contribution from the PSF wings. The default PSF, alignment, and vignetting corrections were used.

During the joint *XMM*–*Newton*/*NuSTAR* observation of 2018, Swift J1756.9–2508 was again detected in the soft state, with a qualitatively identical spectrum to the 2007 (this work) and 2009 (Patruno et al. 2010) *RXTE* observations. Exploiting the energy range of *XMM*–*Newton* we update the estimation of interstellar absorption to a value of  $nH \sim 7 \times 10^{22}$  cm $^{-2}$ . The accretion disc temperature was estimated at  $kT_{in} \sim 1.2$  keV and the temperature of the blackbody component at  $kT_{BB} \sim 2.8$  keV. The non-thermal, power-law-shaped component of the spectrum had a spectral index of  $\Gamma \sim 1.4$  and an exponential drop-off at  $\sim 23$  keV. Despite the similarity in the spectral continuum, the prominent Fe  $K\alpha$  emission line detected in both the 2007 and 2009 *RXTE* observations had disappeared in the 2018 observation. We place a  $1\sigma$  upper limit of 7.36 eV for the EW of the iron  $K\alpha$  emission line. The model for the continuum emission yielded a reduced  $\chi^2$  value of 1.03 for 3141 d.o.f.. In Fig. 6 we present the data-to-ratio plot of the *XMM*–*Newton* observation together with the 2007 *RXTE* observation, for comparison and, in Fig. 7, that of the joint broadband data. The source luminosity during the 2018 *XMM*–*Newton*/*NuSTAR* observation was  $\approx 4 \times 10^{36}$  erg s $^{-1}$ , calculated in the 0.50–30 keV range and assuming the distance of

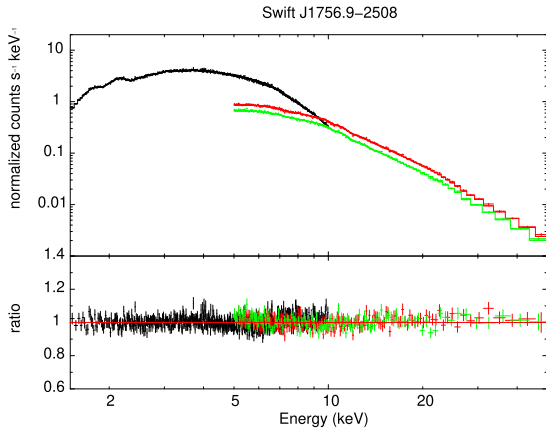


**Figure 7.** Normalized counts versus energy and ratio of the data to the continuum model for the 2018 *XMM-Newton/NuSTAR* observation Swift J1756.9–2508. The data have been re-binned for clarity; the 1–50 keV energy range is shown.

8.5 kpc. All values of the best-fitting parameters along with errors in the 90 per cent confidence range are presented in Table 3.

### 3 DISCUSSION

We have analysed the high-energy spectra of 4U 1543–624 and Swift J1756.9–2508 during different periods in their observational history. In all observations, the sources appeared to have been captured in an accretion-dominated (*soft*) state. In this state, the accretion disc is extending close to the compact object (in our case an NS) and the observed spectrum is dominated by thermal emission. We have modelled the spectra of both sources using a combination of a multicolor disc blackbody and a blackbody model with a very high temperature (with the addition of a non-thermal tail when required). The choice for this model is motivated by the well established theoretical framework for accretion on to low-*B* NSs and the formation of a hot optically thick layer of material on the NS surface, known as the boundary layer (e.g. Sunyaev & Shakura 1986; Popham & Sunyaev 2001; Gilfanov, Revnitsev & Molkov 2003). The boundary layer is a transition region between the rapidly spinning accretion disc and the NS that is rotating at a slower rate. The optically thick matter that accumulates on the NS surface is predicted to have a temperature of  $>1$  keV, producing thermal emission that accounts for a significant fraction of the total accretion luminosity.

The most notable narrow emission feature detected on top of the spectral continuum (in the energy range  $\lesssim 10$  keV) was a prominent and broad Fe K  $\alpha$  emission line, centred at  $\approx 6.5$ – $6.6$  keV. The iron emission line is observed in both sources during two different instances and in the case of 4U 1543–624 by two different instruments. In general, the presence of iron emission is a common characteristic in the X-ray spectra of accreting compact objects and is the result of ‘reflection’ of X-rays from the surface of the accretion disc (e.g. see Done, Gierliński & Kubota 2007; Gilfanov 2010, and references therein). Namely, hard X-rays are reflected off the accretion disc, and the reflected component is registered along with the primary disc emission. The Fe K  $\alpha$  line is the result of this reflection, as a fraction of high energy photons – that are ‘absorbed’ by iron atoms – are re-emitted at the energy corresponding to the electron transition from the 2p orbital of the L-shell to the innermost K-shell. While the detection of iron fluorescence in X-ray spectra of LMXBs – such as 4U 1543–624 and Swift J1756.9–2508 – is a

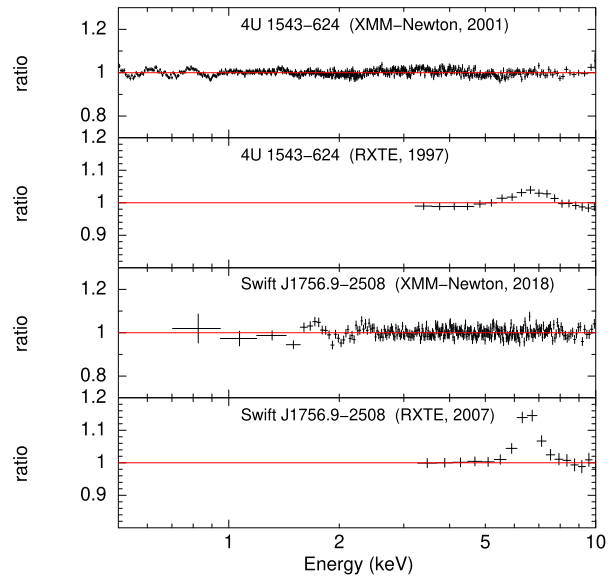


**Figure 8.** Data-to-model ratio plots for the two sources with a variable Fe K  $\alpha$  emission line.

frequent and expected occurrence, a much more extraordinary event, is the fact that the emission line seems to have disappeared during some of the available observations (see Fig. 8 for data-to-model ratio plots indicating the disappearance of the emission line in the spectra of both sources, during different observing dates).

#### 3.1 Fe K $\alpha$ line variability and the spectral state of the two UCXBs

The spectral continuum of 4U 1543–624 displays a remarkable consistency throughout all available observations, which have been carried out over two decades. Within our interpretation for the origin of the emission in 4U 1543–624, the bulk of the 0.5–10 keV emission appears to be produced by an accretion disc with a temperature of  $\sim 0.6$ – $0.8$  keV and an inner disc radius of the order of 10 km, and an additional, hot thermal source with an  $\sim 1.5$ – $1.8$  keV temperature. The luminosity of the source has varied moderately by a factor of up to 25 per cent, and any minor variability of its spectrum is mostly manifested in the relative flux of each spectral component. Over the course of its observational history, the spectrum of 4U 1543–624 has been modelled using a variety of different models, including blackbody, disc blackbody models, power-law components with high energy cutoffs below 10 keV, as well as broken power laws with two spectral indexes, or more complex X-ray reflection models (e.g. Farinelli et al. 2003; Schultz 2003; Madej & Jonker 2011; Madej et al. 2014). We argue that the simplicity and long term consistency of our chosen model, combined with the fact that it yields physically realistic estimations of key emission parameters (see below), favours our interpretation for the origin of the source emission. During the 1997 *RXTE* observation, we detected a Fe K  $\alpha$  emission line with an EW of  $\sim 100$  eV, which is not present in either the *Chandra* or *XMM-Newton* spectra with a stringent EW upper limit of 6.13 and 2.86 eV, respectively. The line is detected again in the 2017 *NICER* observation with an EW of  $\sim 60$  eV.

For Swift J1756.9–2508, we consider the same interpretation for the origin of the spectral continuum as for 4U 1543–624. This source also appears to have a stable spectral shape during its three recorded outbursts (in this work, we present the first and third outburst; for the

second outburst, see Patruno et al. 2010). However, we do note the detection of minor, in the temperatures of the thermal components;  $kT_{\text{in}} \sim 0.96$  keV in *RXTE* versus  $kT_{\text{in}} \sim 1.24$  keV in the *XMM–Newton/NuSTAR* data (the values are consistent within the 90 per cent range) and 2.3 keV versus 2.8 keV for the thermal emission (the values are consistent in the  $2\sigma$  range) and a moderate variability (order of  $\times 7$  in the relative flux of the hot thermal component between observations. Nevertheless, as in the case of 4U 1543–624, the most striking difference between the Swift J1756.9–2508 spectrum of 2018 and the one of 2007 is the disappearance of the prominent Fe K  $\alpha$  line. Namely, the bright iron emission line detected in the 2007 *RXTE* observation with an EW of  $\sim 170$  eV is not detected during the 2018 *XMM–Newton/NuSTAR* observation with an EW upper limit of 7.36 eV. We also note a 25 per cent variation of the total source flux.

A crucial factor for establishing the reliability of our interpretation of the spectral continuum in both sources – and more importantly for identifying the cause for the notable variability of the strength of the iron emission line – is the rigorous estimation of true values of its spectral parameters, i.e. the temperature and inner radius of the accretion disc. To further assess the plausibility of our best-fitting estimations, it is also important to compare our findings with theoretical expectations. In two of the Swift J1756.9–2508 observations (*RXTE* and *NICER*), the best value of the inner disc radius is measured in the  $\sim 8$ – $10.5$  km range, while for Swift J1756.9–2508, they range between  $\sim 4$  and  $\sim 6$  km. These estimations lie below the value of the NS radius that is  $\sim 9$ – $5$  km depending on the equation of state of the NS (e.g. Özel & Freire 2016, and references therein), and therefore appear to be unrealistically small. Nevertheless, we note that in all tabulated values, we have not considered the necessary corrections of the thermal component parameters due the spectral hardening expected from the high plasma temperature. Correcting the inner radius estimations, assuming a moderate value of 1.8 for the spectral hardening factor (see Section 2.1), yields  $R_{\text{in}}$  values in the  $\sim 15$ – $45$  km for the entire set of observations, which is the typical size for an accreting low- $B$  NS in the soft state.

Therefore within this framework, the presence of iron K  $\alpha$  fluorescence in the spectra of 4U 1543–624 and Swift J1756.9–2508 is the result of illumination of the inner accretion disc by the boundary layer emission. Since the iron line is produced by X-ray reflection, its shape and strength are highly sensitive to the geometrical arrangement between the source of the primary emission (e.g. the boundary layer) and the accretion disc. Modification of the size and temperature of the emitting region, the inner radius of the accretion disc, and the direction of the hard X-ray emission will affect the size and location of the illuminated region of the disc. These effects will become especially pronounced in case of spectral state transition towards the so called ‘hard’ state of accretion, were the disc recedes from the central source, giving way to the formation of an extended region of advection-dominated, optically thin radial flow. This ‘corona’ consisting of very hot electrons produces copious amounts of non-thermal photons, resulting in a spectrum that is dominated by the power-law shaped component. Therefore, state transitions can have profound effects on the strength of the iron emission line (e.g. Cackett et al. 2010; Ng et al. 2010; Kolehmainen, Done & Díaz Trigo 2014). Similar effects can also be observed in accreting highly magnetized NS (i.e. high- $B$ , X-ray pulsars), where variations in the accretion rate affect the size of the magnetosphere, the inner disc radius, and the direction of the pulsar beam, resulting in pronounced variability in the iron line strength (e.g. Koliopanos & Gilfanov 2016). Therefore, the striking variability of the iron line as observed in 4U 1543–624 and Swift J1756.9–2508 are expected to occur in tandem with major modification of the spectral continuum and/or the source luminosity.

However, one of the main findings of our analysis is the notable stability of the spectrum and luminosity of both sources throughout the different observations with or without the presence of iron K  $\alpha$  fluorescence. This suggests that the attenuation of the iron line is not caused by a ‘macroscopic’ transition in the accretion state of the source, but is likely the result of a more subtle microscopic process. To our knowledge, such remarkable emission line variability in an otherwise stable X-ray binary has not been previously observed. However, the possibility of this phenomenon had been hypothesized by Koliopanos et al. (2013) for UCXBs with C/O-rich donors.

### 3.2 Variability of the Fe K $\alpha$ line in UCXBs with C/O-rich donors

In Koliopanos et al. (2013), it was demonstrated that the Fe K  $\alpha$  emission line in the spectra of UCXBs with C/O-rich donors is expected to be strongly attenuated, with expected values of the EW to be less than 10 eV. The attenuation of the iron emission line is primarily due to the presence of overabundant oxygen<sup>7</sup> in the accreting material. Namely, contrary to accretion discs with solar-like abundance, in the C/O-rich discs, absorption of photons with energies equal to or higher than the ionization threshold of iron ( $E \approx 7.1$  keV), is dominated by oxygen rather than by iron. This results in the strengthening of the oxygen emission line (centred at  $\sim 0.68$  keV) and the strong attenuation of the iron line. More specifically, after running the MCMC code of Koliopanos et al. (2013) for an incident 1-keV blackbody spectrum and for a range of observer viewing angles between  $10^\circ$  and  $50^\circ$ , we find that an O/Fe ratio of at least 50 times the solar value is required to explain the absence of a Fe K  $\alpha$  line at an EW upper limit of 8 eV. This *screening* effect will hold as long as the oxygen in the accretion disc is not fully ionized.

The ionization state of elements in the disc was not self-consistently treated in the model developed by Koliopanos et al. (2013). However, the effects of the ionization state of the disc were discussed – under a set of specific assumptions. Namely, we considered that the ionization state of the disc is determined solely by heating due to viscous dissipation as illustrated in the Shakura & Sunyaev (1973) formulation. We have ignored the effects of disc irradiation by assuming the conditions described in the Nayakshin, Kazanas & Kallman (2000) analysis, predicting the formation of a thin, fully ionized layer on the disc surface that is dominated by X-ray illumination, while the temperature of deeper disc layers remain unaffected. Within this regime, Koliopanos et al. (2013) roughly estimated that during the *soft state* and for a mass accretion rate ( $\dot{M}$ ) corresponding to  $L_X$  of the order of a few  $\times 10^{37}$  erg s<sup>-1</sup>, oxygen could become fully ionized in the accretion disc of an UCXB, thus cancelling its *screening* effect on the iron line. Within this framework, the iron line variability in UCXBs is luminosity dependent.

More specifically assuming an optically thick, geometrically thin disc following the Shakura–Sunyaev  $\alpha$ -disc model, the effective temperature of the disc is given by

$$T_{\text{eff}} = \left( \frac{3GM\dot{M}}{8\pi\sigma r_0^3} \right)^{1/4} \left( \frac{r_0}{r} \right)^{3/4} \left( 1 - \sqrt{r_0/r} \right)^{1/4}, \quad (3)$$

where  $\sigma = 5.67 \times 10^{-5}$  erg cm<sup>-2</sup> s<sup>-1</sup> K<sup>-4</sup> is the Stefan–Boltzmann constant,  $M$  is the mass of the accretor ( $\sim 1.4 M_\odot$  for a neutron star),  $\dot{M}$  the mass accretion rate, and  $r_0$  is the inner radius of the disc,

<sup>7</sup>The maximum value of the O/Fe ratio corresponding to the chemical composition of a C/O white dwarf – in which all hydrogen and helium has been converted into carbon and oxygen – is  $\approx 77$  times the solar value.

which, in the case of the soft state of a neutron star, is close to its radius. For a moderate  $\dot{M}$ , (corresponding to  $L \approx 2 \times 10^{37}$  erg s<sup>-1</sup>), the temperature of the inner parts of the disc (up to  $15 r_g$ ; where  $r_g$  is the gravitational radius  $r_g = GM/c^2$ ) will range within  $(5-8) \times 10^6$  K. In addition to heating due to viscous dissipation, if the accretion disc forms a boundary layer near the surface of the NS, it will cause a dissipation of the kinetic energy of the inner disc rings, which, in turn, will result in the inflation and heating of the innermost part of the disc (Inogamov & Sunyaev 1999). Inogamov & Sunyaev (1999) calculate that the inner disc will be heated to  $\sim 10^7$  K as the boundary layer forms. When the temperature reaches  $\sim 10^7$  K – and assuming that the disc plasma is in collisional ionization equilibrium, in a coronal approximation – 90–100 per cent of oxygen will be fully ionized (Shull & van Steenberg 1982).

The above analytical estimations demonstrate, that for typical conditions that can be met by moderately bright UCXBs, it is very likely that a considerable fraction of the inner accretion disc can reach a high enough temperature for all oxygen to become fully ionized. Although there is considerable uncertainty in the distance estimation for our two sources – different estimations place 4U 1543–624 anywhere between 1.4–11.5 kpc (Bailer-Jones et al. 2018; Serino et al. 2018), while Swift J1756.9–2508 is assumed to be at a distance of 8.5 kpc due to its proximity to the galactic bulge – we can robustly place both sources in the in the  $10^{36}$ – $10^{37}$  erg s<sup>-1</sup> range. From our analysis, the colour-corrected, maximum disc temperature obtained by the `diskbb` model, during the epochs when the line is detected is  $\sim 5 \times 10^6$  K for 4U 1543–624 and  $\sim 8 \times 10^6$  K for Swift J1756.9–2508 (we note that `diskbb` is only an approximation of the full Shakura & Sunyaev 1973 treatment).

The X-ray luminosity of both sources is marginally lower than the rough threshold of  $\log(L_X) \sim 37.5$  suggested by Koliopanos et al. (2013). Similarly the spectroscopic estimations of the accretion disc lies below the  $\approx 1$  KeV value for the full ionization of 100 per cent of the disc oxygen, but only marginally so. If we also take into account that the state-of-the-art Monte Carlo simulations of X-ray reflection (e.g. García & Kallman 2010; García, Kallman & Mushotzky 2011; García et al. 2013) indicate that X-ray irradiation can increase the disc ionization at deeper layers than the Nayakshin et al. (2000) estimations, we can reasonable assume that our sources lie exactly at the threshold between having most of their oxygen partially ionized (suppression of Fe K $\alpha$  line) to fully ionized (re-appearance of Fe K $\alpha$  line). We note that in both cases the overabundance of oxygen expected in the C/O-rich disc (50–80 times the Solar value) ensures the presence of notable a O VIII fluorescent line even when most of it becomes fully ionized (although the actual detection of such a feature depends on multiple additional parameters; see discussion in Koliopanos et al. 2013). Indeed, this line is detected at  $\sim 0.68$  keV in 4U 1543–624, where the low absorption allows for its detection (see Fig. 1 and refer to Ludlam et al. 2019 for an analysis of the *NICER* observation).

We argue that the disappearance of the iron line occurring within an otherwise non-variable spectral state, is a strong indication that 4U 1543–624 and Swift J1756.9–2508 are both C/O-rich UCXBs observed at the threshold at which the screening of the iron line ceases to exist. As a result of this precarious state, subtle variations on the parameters of the accretion process, may lead to an increase in the fraction of fully ionized oxygen, evidenced by the reappearance of the iron emission line. Besides this striking variability in the Fe K $\alpha$  line flux, the change in the ionization state has negligible effects on other observables. We consider this discovery an encouraging result with respect to the Koliopanos et al. (2013) theoretical predictions on X-ray reflection off H-poor discs in UCXBs and their potential use

as a diagnostic of the composition of the accretion disc and donor star in these sources.

## 4 SUMMARY AND CONCLUSIONS

We have analysed multiple observations of known UCXBs 4U 1543–624 and Swift J1756.9–2508, carried out at different eras within a 20-yr period and with different instruments. We have demonstrated that both sources (one is a persistent and the other a transient source), exhibit a remarkable stability of the shape of their spectral emission and their X-ray luminosity (during outburst). Nevertheless, we also detected a pronounced difference in the spectral characteristics at different epochs, in the form of a striking variability in the strength of the iron K $\alpha$  emission line. Namely, the emission line is either detected as a prominent feature with an EW of 100–170 eV, or completely disappears with an EW upper limit of less than 8 eV. Based on the stability of the spectral shape and flux of both sources throughout the different observations, and on the values of their spectral parameters, we have attributed the iron line variability to a change in the ionization state of oxygen in the inner accretion disc regions. Namely, subtle variations of the accretion disc parameters can lead to a transition from partially to fully ionized oxygen in the disc, which, in turn, affects the strength of the iron line, as has been predicted for UCXBs with C/O-rich donors by Koliopanos et al. (2013). We argue that this behaviour supports the theoretical arguments of this work and favors the C/O-rich classification of the UCXBs 4U 1543–624 and Swift J1756.9–2508.

## ACKNOWLEDGEMENTS

The French team are grateful to Centre National d’Études Spatiales (CNES) for their support in the work related to *XMM-Newton*, *NuSTAR*, and *NICER*. FK extends his deep gratitude to the referee and editor of this paper, for significantly contributing to its final form, but more importantly for their patience and understanding during a prolonged pause in the refereeing process, which was caused by FK, due to an unforeseen personal issue.

## DATA AVAILABILITY

The observational data underlying this paper are publicly available at the NASA HEASARC archive.<sup>8</sup> Any details with regard to the Monte Carlo source code can be shared on reasonable request to the corresponding author.

## REFERENCES

- Arnaud K. A., 1996, in Jacoby G. H., Barnes J., eds, ASP Conf. Ser. Vol. 101, Astronomical Data Analysis Software and Systems V. Astron. Soc. Pac., San Francisco, p. 17
- Bailer-Jones C. A. L., Rybizki J., Foesneau M., Mantelet G., Andrae R., 2018, *AJ*, 156, 58
- Barret D., 2001, *Adv. Space Res.*, 28, 307
- Bildsten L., Deloye C. J., 2004, *ApJ*, 607, L119
- Bogdanov S. et al., 2019, *ApJ*, 887, L25
- Bult P. et al., 2018a, *ApJ*, 864, 14
- Bult P. M. et al., 2018b, *Astron. Telegram*, 11502, 1
- Cackett E. M. et al., 2009, *ApJ*, 690, 1847
- Cackett E. M. et al., 2010, *ApJ*, 720, 205
- Deloye C. J., Bildsten L., 2003, *ApJ*, 598, 1217

<sup>8</sup><https://heasarc.gsfc.nasa.gov/docs/archive.html>.

- Deloye C. J., Bildsten L., Nelemans G., 2005, *ApJ*, 624, 934
- Done C., Gierliński M., Kubota A., 2007, *A&AR*, 15, 1
- Farinelli R. et al., 2003, *A&A*, 402, 1021
- García J., Dauser T., Reynolds C. S., Kallman T. R., McClintock J. E., Wilms J., Eikmann W., 2013, *ApJ*, 768, 146
- García J., Kallman T. R., 2010, *ApJ*, 718, 695
- García J., Kallman T. R., Mushotzky R. F., 2011, *ApJ*, 731, 131
- Gendreau K. C., Arzoumanian Z., Okajima T., 2012, Proc. SPIE Conf. Ser. Vol. 8443, The Neutron Star Interior Composition Explorer (*NICER*): An Explorer Mission of Opportunity for Soft X-ray Timing Spectroscopy. SPIE, Bellingham, p. 844313
- Gilfanov M., 2010, in Belloni T., ed., Lecture Notes in Physics, Vol. 794, The Jet Paradigm. Springer-Verlag, Berlin, p. 17
- Gilfanov M., Revnitsev M., Molkov S., 2003, *A&A*, 410, 217
- Guillot S. et al., 2019, *ApJ*, 887, L27
- HI4PI Collaboration et al., 2016, *A&A*, 594, A116
- Iben, Iben I., Jr., Tutukov A. V., Yungelson L. R., 1995, *ApJS*, 100, 233
- Inogamov N. A., Sunyaev R. A., 1999, *Astron. Lett.*, 25, 269
- Jahoda K., Markwardt C. B., Radeva Y., Rots A. H., Stark M. J., Swank J. H., Strohmayer T. E., Zhang W., 2006, *ApJS*, 163, 401
- Jones C., 1977, *ApJ*, 214, 856
- Juett A. M., Chakrabarty D., 2003, *ApJ*, 599, 498
- Juett A. M., Chakrabarty D., 2005, *ApJ*, 627, 926
- Juett A. M., Psaltis D., Chakrabarty D., 2001, *ApJ*, 560, L59
- Kolehmainen M., Done C., Díaz Trigo M., 2014, *MNRAS*, 437, 316
- Koliopanos F., Gilfanov M., 2016, *MNRAS*, 456, 3535
- Koliopanos F., Gilfanov M., Bildsten L., 2013, *MNRAS*, 432, 1264
- Koliopanos F., Gilfanov M., Bildsten L., Trigo M. D., 2014, *MNRAS*, 442, 2817
- Koliopanos F., Peault M., Vasilopoulos G., Webb N., 2020, *MNRAS*
- Krimm H. A. et al., 2007, *ApJ*, 668, L147
- Kuiper L., Tsygankov S., Falanga M., Galloway D., Poutanen J., 2018, *Astron. Telegram*, 11603, 1
- Lapidus I. I., Sunyaev R. A., Titarchuk L. G., 1986, *Sov. Astron. Lett.*, 12, 383
- Levine A. M., Bradt H., Cui W., Jernigan J. G., Morgan E. H., Remillard R., Shirey R. E., Smith D. A., 1996, *ApJ*, 469, L33
- Lin D., Remillard R. A., Homan J., 2007, *ApJ*, 667, 1073
- London R. A., Taam R. E., Howard W. M., 1986, *ApJ*, 306, 170
- Ludlam R., Miller J. M., Miller-Jones J., Reynolds M., 2017, *Astron. Telegram*, 10690, 1
- Ludlam R. M. et al., 2018, *ApJ*, 858, L5
- Ludlam R. M. et al., 2019, *ApJ*, 883, 39
- Madej O. K., García J., Jonker P. G., Parker M. L., Ross R., Fabian A. C., Chenevez J., 2014, *MNRAS*, 442, 1157
- Madej O. K., Jonker P. G., 2011, *MNRAS*, 412, L11
- Madej O. K., Jonker P. G., Fabian A. C., Pinto C., Verbunt F., de Plaa J., 2010, *MNRAS*, 407, L11
- Miller J. M., Ludlam R. M., Reynolds M. T., Kuulkers E., Ferrigno C., Bozzo E., 2017, *Astron. Telegram*, 10719, 1
- Mitsuda K., Inoue H., Nakamura N., Tanaka Y., 1989, *PASJ*, 41, 97
- Mitsuda K. et al., 1984, *PASJ*, 36, 741
- Nayakshin S., Kazanas D., Kallman T. R., 2000, *ApJ*, 537, 833
- Nelemans G., Jonker P. G., Marsh T. R., van der Klis M., 2004, *MNRAS*, 348, L7
- Nelemans G., Jonker P. G., Steeghs D., 2006, *MNRAS*, 370, 255
- Nelson L. A., Rappaport S. A., Joss P. C., 1986, *ApJ*, 311, 226
- Ng C., Díaz Trigo M., Cadolle Bel M., Migliari S., 2010, *A&A*, 522, A96
- Özel F., Freire P., 2016, *ARA&A*, 54, 401
- Patruno A., Altamirano D., Messenger C., 2010, *MNRAS*, 403, 1426
- Podsiadlowski P., Rappaport S., Pfahl E. D., 2002, *ApJ*, 565, 1107
- Popham R., Sunyaev R., 2001, *ApJ*, 547, 355
- Rappaport S., Joss P. C., 1984, *ApJ*, 283, 232
- Revnitsev M. G., Suleimanov V. F., Poutanen J., 2013, *MNRAS*, 434, 2355
- Rothschild R. E. et al., 1998, *ApJ*, 496, 538
- Sanna A. et al., 2018, *MNRAS*, 481, 1658
- Savonije G. J., de Kool M., van den Heuvel E. P. J., 1986, *A&A*, 155, 51
- Schultz J., 2003, *A&A*, 397, 249
- Serino M. et al., 2018, *Astron. Telegram*, 11302, 1
- Shakura N. I., Sunyaev R. A., 1973, *A&A*, 24, 337
- Shimura T., Takahara F., 1995, *ApJ*, 445, 780
- Shull J. M., van Steenberg M., 1982, *ApJS*, 48, 95
- Sibgatullin N. R., Sunyaev R. A., 2000, *Astron. Lett.*, 26, 699
- Sunyaev R. A., Shakura N. I., 1986, *Sov. Astron. Lett.*, 12, 117
- Tutukov A. V., Yungelson L. R., 1993, *Astron. Rep.*, 37, 411
- Verbunt F., van den Heuvel E. P. J., 1995, in Lewin W. H. G., van Paradijs J., van den Heuvel E. P. J., eds., Formation and evolution of neutron stars and black holes in binaries, X-ray Binaries. Cambridge University Press, Cambridge, p. 674
- Wang Z., Chakrabarty D., 2004, *ApJ*, 616, L139
- Werner K., Nagel T., Rauch T., Hammer N. J., Dreizler S., 2006, *A&A*, 450, 725
- White N. E., Stella L., Parmar A. N., 1988, *ApJ*, 324, 363
- Wilms J., Allen A., McCray R., 2000, *ApJ*, 542, 914
- Yungelson L. R., Nelemans G., van den Heuvel E. P. J., 2002, *A&A*, 388, 546
- Zimmerman E. R., Narayan R., McClintock J. E., Miller J. M., 2005, *ApJ*, 618, 832

This paper has been typeset from a  $\text{\TeX}/\text{\LaTeX}$  file prepared by the author.